INL/RPT-24-80975-Revision-0

Design, Fabrication and Testing of Surveillance Test Articles for MSR Materials Degradation Management

September 2024

Xinchang Zhang, Heramb Prakash Mahajan, Michael D McMurtrey

Changing the World's Energy Future

Idaho National Laboratory

INL is a U.S. Department of Energy National Laboratory operated by Battelle Energy Alliance, LLC

INL/RPT-24-80975-Revision-0

Design, Fabrication and Testing of Surveillance Test Articles for MSR Materials Degradation Management

Xinchang Zhang, Heramb Prakash Mahajan, Michael D McMurtrey

September 2024

Idaho National Laboratory
Idaho Falls, Idaho 83415

http://www.inl.gov

Prepared for the
U.S. Department of Energy
Under DOE Idaho Operations Office
Contract DE-AC07-05ID14517

Design, Fabrication, and Testing of Surveillance Test Articles for Molten-Salt Reactor Materials Degradation Management

INL/RPT-24-80975

Advanced Reactor Technologies

SEPTEMBER 2024

Xinchang Zhang, Heramb Mahajan, and Michael McMurtrey

Idaho National Laboratory

Idaho National Laboratory

Battelle Energy Alliance manages INL for the U.S. Department of Energy's Office of Nuclear Energy

INL/RPT-24-80975

Design, Fabrication, and Testing of Surveillance Test Articles for Molten-Salt Reactor Materials Degradation Management

Xinchang Zhang, Heramb Mahajan, and Michael McMurtrey
Idaho National Laboratory

September 2024

Idaho National Laboratory
Advanced Reactor Technologies
Idaho Falls, Idaho 83415

http://www.art.inl.gov

Prepared for the
U.S. Department of Energy
Office of Nuclear Energy
Under DOE Idaho Operations Office
Contract DE-AC07-05ID14517

Page intentionally left blank

INL ART Program

Design, Fabrication, and Testing of Surveillance Test Articles for Molten-Salt Reactor Materials Degradation Management

INL/RPT-24-80975

September 2024

Technical Reviewer: (Confirmation of mathematical accuracy, and correctness of data and appropriateness of assumptions.)

Ninad Mohale — 9/24/2024

Ninad Mohale
Materials Engineer

Date

Approved by:

9/24/2024

Michael E. Davenport
ART Project Manager

Date

Travis Mitchell — 9/24/2024

Travis R. Mitchell
ART Project Manager

Date

9/24/2024

Michelle T. Sharp
INL Quality Assurance

Date

Page intentionally left blank

ABSTRACT

This report details the design, fabrication, and testing of surveillance test articles designed to assess material damage in reactor-relevant environments for effective degradation management. Two types of surveillance test articles of reduced sizes were developed, based on design algorithms and finite-element modeling: a welded and an interlocking design. A furnace heating setup was adopted for validation testing to apply multiple thermal-cyclic loading profiles on the test articles with a temperature range of 500 to 700°C while the strain response was monitored using a digital image correlation (DIC) technique. The testing results demonstrated successful capture of expected strain range for the welded design while machining tolerance should be improved to engage strain coupling in the interlocking design. Mid-term (500 hours) and long-term (1500 hours) cyclic tests were conducted on welded test articles. A constant strain range of ~0.6% was observed at the specimen with testing under 500 hours while a gradual decrease of strain at specimen was observed after 500 hours. Non-destructive evaluation through X-ray computed tomography (XCT) confirmed that microcracks in the welds at specimen-driver joints after cyclic test caused the strain change. Creep testing of the specimen after long-term cyclic test revealed a shorter creep life than expected. A multiprofile cyclic test was also conducted on a test article and demonstrated consistent strain response under different temperature ramp rates. The report also briefly discusses the challenges and future research efforts to advance test-article development for material surveillance.

Page intentionally left blank

ACKNOWLEDGMENTS

This research was sponsored by the U.S. Department of Energy (DOE) under Contract No. DE-AC07-05ID14517 with Idaho National Laboratory (INL), which is managed and operated by Battelle Energy Alliance. Programmatic direction was provided by the Office of Nuclear Research Deployment of the DOE Office of Nuclear Energy (NE).

The authors gratefully acknowledge the support provided by Sue Lesica of DOE-NE, federal lead for Advanced Materials, Advanced Reactor Technologies (ART) Program, Janelle Eddins of DOE-NE, federal manager, ART Molten Salt Reactors (MSR) Campaign, and Patricia Paviet of Pacific Northwest National Laboratory, national technical director, ART MSR Campaign.

The authors also thank the assistance of David Cottle, Austin Matthews, Tate Patterson, Asa Monson, and Joel Simpson of INL for experimental support.

Page intentionally left blank

CONTENTS

FIGURES

TABLES

ACRONYMS

ANL	Argonne National Laboratory
ART	Advanced Reactor Technologies (Program)
ASME	American Society of Mechanical Engineers
ASTM	American Society for Testing and Materials
CTE	coefficient of thermal expansion
DIC	digital-image correlation
DED	Directed Energy Deposition
DOE	U.S. Department of Energy
EDM	Electric Discharge Machining
FEM	Finite Element Modeling
HBB	Subsection HB, Subpart B
INL	Idaho National Laboratory
ISTA	interlocking surveillance test article
LWR	Light Water Reactor
LVDT	Linear Variable Differential Transformer
MSR	Molten Salt Reactor
NE	Nuclear Energy
NRC	Nuclear Regulatory Commission
SCC	Structures Components and Systems
TZM	Titanium-Zirconium-Molybdenum
WSTA	Welded Surveillance Test Article
XCT	X-ray Computed Tomography

Page intentionally left blank

Design, Fabrication, and Testing of Surveillance Test Articles for Molten-Salt Reactor Materials Degradation Management

1. INTRODUCTION

Molten-salt reactors (MSRs) are a type of Generation-IV nuclear reactor that operate at temperatures ranging from 500 to 700°C. In MSR designs, molten salt may serve as the coolant or coolant with dissolved fuel in the primary loop. Typical reactor operation often involves thermal transients driven by fluctuations in power demand. As a result, structures, systems, and components (SSCs) that form the primary coolant boundary are exposed to highly corrosive and irradiative environments at elevated temperatures with thermal transients. These conditions can accelerate material degradation and damage accumulation through the interaction of mechanical stresses, corrosion, and irradiation. These coupled degradation mechanisms are influenced by factors such as salt chemistry, material composition, operation-temperature range, and degree of exposure to radiation. However, there are limited data on the combined effects of corrosion, irradiation, and mechanical damage on materials used for MSR-component construction, due to the challenges and expenses associated with pairing corrosion, stress, and irradiation in a single test at elevated temperature. Collecting degradation data from each fluid type separately is impractical, highlighting the need for a comprehensive material-surveillance program. Such a program would gather in situ data on material degradations to assess the accumulated damage in SSCs and facilitate the timely licensing of MSRs by ensuring a means of collecting missing materials information during operation.

The American Society of Mechanical Engineers (ASME) Boiler and Pressure Vessel Code, Section III, Division 5, provides construction rules for SSCs in high-temperature nuclear applications (2023a). While Section III, Division 5, Subsection HB, Subpart B, outlines allowable stresses and design curves for high-temperature materials, it does not account for material degradation due to corrosion, erosion, or irradiation. To ensure component integrity, it is essential to consider these coupled damage mechanisms and adopt stress-reduction factors accordingly.

Recent draft-interim staff guidance from the U.S. Nuclear Regulatory Commission (NRC) suggests that reasonable structural-integrity assurance could be achieved through monitoring and surveillance (2023b). The proposed Materials Surveillance Program aims to collect in situ data on material degradation within nuclear reactors, supporting both design and licensing processes. The program will periodically assess changes in material properties due to neutron radiation, aiming to evaluate component life and structural integrity. This approach has historical precedent in the monitoring changes in fracture toughness of reactor pressure vessel steels, as well as some internal support components, in light-water reactors (LWRs).

While the Material Surveillance Program for Generation-IV reactors is conceptually similar to the in-situ programs used for LWRs, the key challenge lies in the Generation-IV environment. Cyclic loads at elevated temperatures can cause mechanical degradation due to creep-fatigue interactions, which makes assessing these loads in an in-situ environment particularly difficult. The American Society for Testing and Materials (ASTM) E531-2023, “Standard Practice for Surveillance Testing of High-Temperature Nuclear Component Materials,” describes surveillance-testing practices, but does not provide guidance on applying passively actuated cyclic loads on samples during testing.

This gap in testing methodologies underscores the need for an in situ, passively loaded testing methodology. Previous work has laid the groundwork for developing material-surveillance technology, including the design and validation of various types of test articles under different cyclic-loadings (McMurtrey et al. 2022, Messner, Momozaki, and Boron 2022, Messner and Sham 2021, Messner et al.

2021, Messner et al. 2020). This report outlines the continued effort in developing and testing surveillance test articles, the adopted design strategies and strain measurements obtained through digital-image correlation (DIC) techniques under different types of cyclic heating profiles during surveillance testing. Additionally, the report discusses the design of welded and interlocking test articles, along with key observations from these tests. Further efforts to advance surveillance programs for materials degradation assessment for complex reactor environments are discussed.

2. SURVEILLANCE TEST-ARTICLE DESIGN

The surveillance test article was designed as a bimetal configuration, consisting of two materials: the material under surveillance (referred to as the "specimen") and a second material with a lower coefficient of thermal expansion (CTE), known as the "driver." Figure 1 provides a schematic representation of the key aspects of this design, which involves three main components: the specimen, the driver, and a third piece called the "column." The specimen and driver are connected in series while the column is not directly connected to this assembly. Both the specimen and column are fixed at Location 1, with Location 2 remaining free. At room temperature, the total length of specimen-driver assembly is equal to the length of the column. As the temperature increases, a thermal-expansion mismatch occurs between the specimen-driver assembly and the column, leading to differential expansion rates. By connecting the specimen-driver assembly to the column at Location 2 to maintain displacement compatibility, this thermal mismatch can serve as a driving force to apply temperature-dependent passive loads on the specimen. Consequently, cyclic loads are applied to the specimen through this connection, as shown in Figure 1. This passive-loading technique is a fundamental feature of the surveillance test-article design.

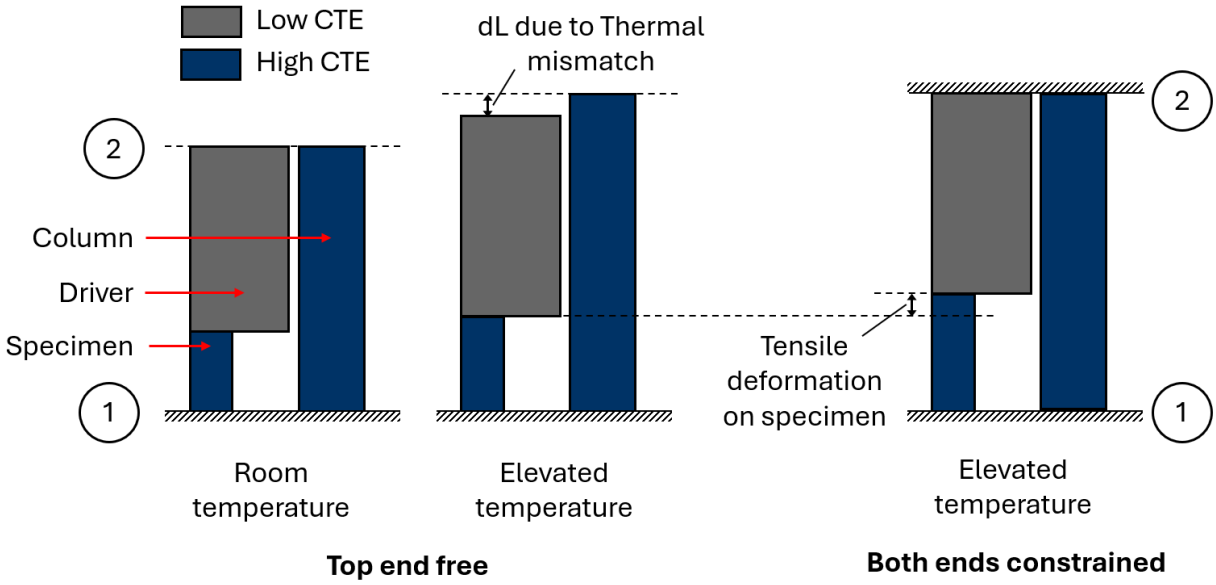

Figure 1. Schematics showing the driver, specimen, and column of the test article and the passive loading of specimen through thermal expansion mismatch.

The key characteristics of an ideal test article design are outlined below. These requirements govern the overall design process.

1. Small size. A smaller test article minimizes the volume of material activation by neutron irradiation and reduces disruption to fluid flow within the system.
2. Connection. The design must account for the limitations of bimetal welding, especially under cyclic loads at elevated temperature. Hence, compatible materials should be chosen for welding, or an alternative connection technique that avoids welding should be used.

3. Thermal Expansion Mismatch. A larger difference in the CTE of the materials allows for a more-compact design. Thus, the driver material should have the lowest possible expansion coefficient.
4. Creep Strength of the Driver. The driver material must withstand environmental conditions and applied loads without degradation. It should also possess greater resistance to creep deformation than the specimen material.

The surveillance test-article design originated from the concept of the simplified model (Wang, Sham, and Jetter 2014). This model captures such key component characteristics as strain range and elastic follow up. A three-bar model was used as the foundation for developing the test-article design. The design strategy to achieve the desired characteristics is outlined below.

1. Design Parameter Selection. Key design parameters include strain range and elastic follow up. The goal is to develop a test article that can be effectively tested within a reasonable timeframe using standard laboratory apparatus.
2. Test Article Geometry Optimization. Previous work by Argonne National Laboratory (ANL) demonstrated that the three-bar model successfully captures the critical characteristics of the surveillance test article (Messner, Momozaki, and Boron 2022, Messner and Sham 2021, Messner et al. 2021, Messner et al. 2020). This model, coupled with a genetic algorithm and constraints, was used to optimize the dimensions of the specimen, driver, and column to achieve the target design parameters. This process yielded the optimal widths and lengths for each component.
3. Detailed Analysis. A finite element model (FEM) was created using the optimized dimensions from Step 2, including a simulation of corners and detailed geometries near load-transfer regions to capture the local material response. Perfect contact was assumed between the specimen and driver, as well as between the driver and column. Two types of specimens were designed: one with welded surveillance test articles (WSTA), where the load is transferred through weld lines, and another with interlocking surveillance test article (ISTA), as shown in Figure 2.

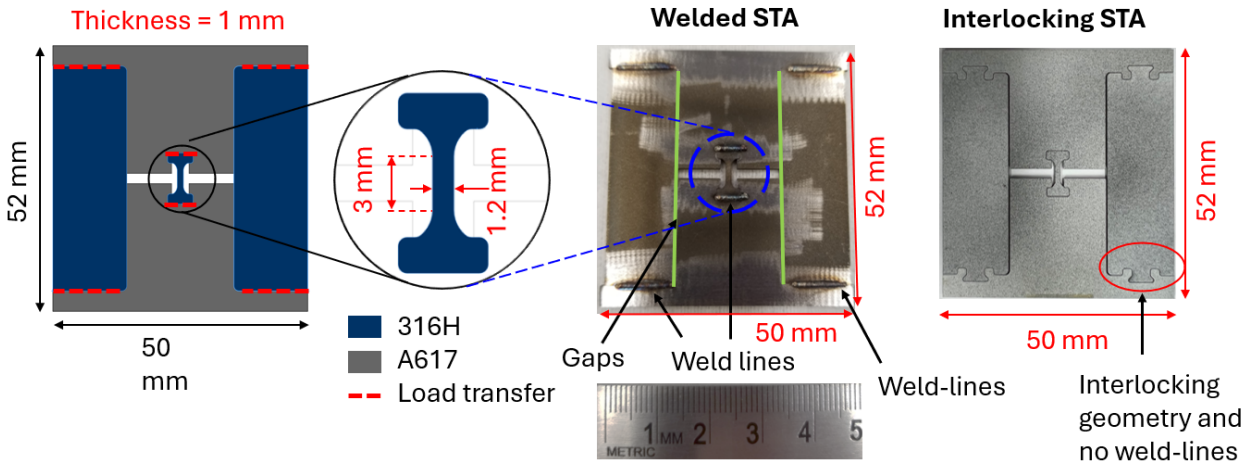

Figure 2. Surveillance test article designs showing welded and interlocking test article geometries.

To support the material surveillance technology, three experimental validation tests were planned, as illustrated in Figure 3.

1. Case One. Surveillance test articles are subjected to thermal cycles until either a drop in strain range or the appearance of microcracks in the specimen is observed. The occurrence of either is considered to indicate specimen failure.

2. Case Two. Partial thermal cycles are applied to the test articles such that the accumulated damage fraction in the specimen remains less than one. Afterward, a specimen is machined from the test article and subjected to pure creep testing. This creep testing provides valuable data on creep rates and the remaining creep life of the sample, which is essential to calculate the damage fraction accumulated during the partial thermal cycles.

3. Case Three. A pure creep test is conducted on the specimen, serving as a baseline for comparison with the other cases.

The data collected from these experiments will be used to evaluate the material-surveillance approach and support the development of analytical procedures to assess the remaining life of the specimen.

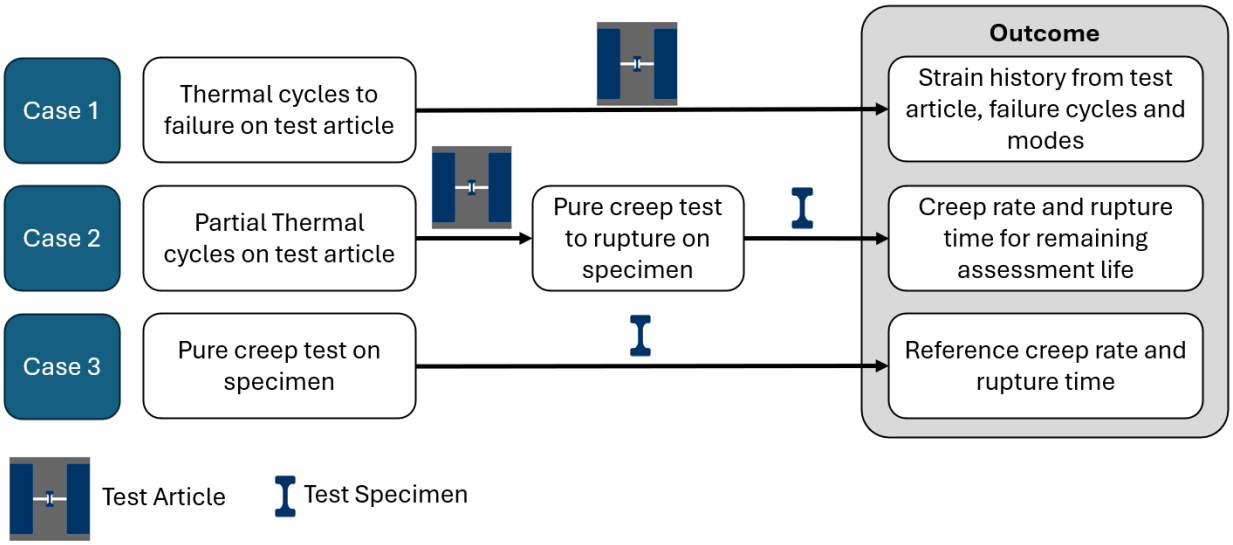

Figure 3. Experimental strategy to support evaluation of the material surveillance technology.

3. TESTING OF SURVEILLANCE TEST ARTICLES

3.1. Experimental Setup

3.1.1. Experimental Setup with Furnace Heating

A tube-furnace heating setup specifically designed for this research, as illustrated in Figure 4, was used to apply thermal cycling on the test articles. Simultaneously, the strain evolution of the test articles was monitored using an updated DIC system. The furnace setup was configured based on prior knowledge to mitigate heat-haze effect on DIC images caused by the convection of hot air mixing with ambient air (Mahajan et al. 2023). As illustrated in Figure 4, the tube furnace features a quartz window at the end of the furnace to minimize air convection at the camera viewport. Additionally, a fan was used to ensure uniform air mixing along the optical path to reduce differences in the refractive index. The high-temperature black-body radiation from the test article significantly affects the grayscale values captured by the camera. To mitigate this issue, monochromatic blue light was adopted to illuminate the speckled surface, and a blue-band-pass filter was mounted on the camera to reduce black-body radiation into the camera. A Type K thermocouple attached to the sample recorded the sample temperature for furnace calibration. It was found that the sample temperature was ~20–25°C lower than the furnace controller's setpoint. Therefore, the furnace was programmed to accommodate this temperature offset. Furthermore, a fixture was designed to securely hold the test article in place during thermal cycling without introducing stress to the specimen.

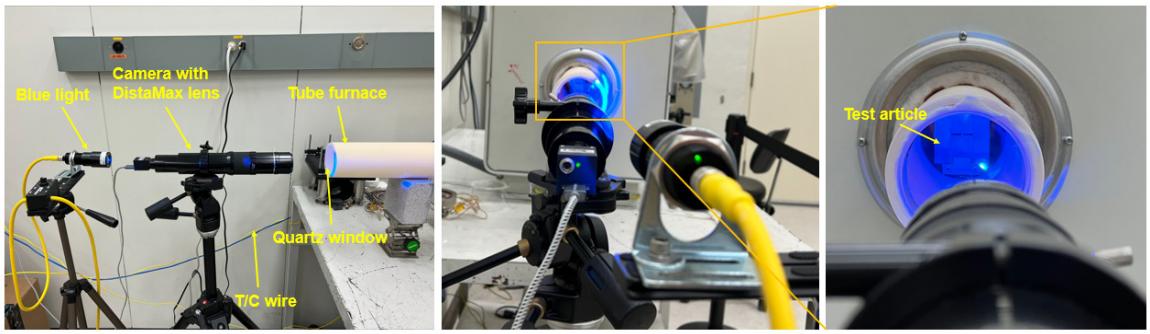

Figure 4. (a) Side view and (b) front view of the tube furnace heating setup with (c) a WSTA in testing. DIC imaging quality was enhanced with quartz window viewport, fan (not shown), and blue light/filter.

3.1.2. Digital Image Correlation

DIC is a non-contact measurement technique that enables precise displacement measurements and strain mapping. The DIC technique works by correlating images of a deformed sample with a reference image of the undeformed sample. The DIC algorithm detects changes in the distance between speckle patterns and creates a displacement map from which strain can be derived. Because DIC relies on image analysis, the quality of the speckle pattern is crucial for accurate measurements. Key factors for a high-quality speckle pattern include: (1) random speckles that form distinct patterns, (2) speckles of appropriate sizes relative to the sample and area of interest, (3) strong adhesion of the speckle pattern to the sample to ensure synchronized deformation, (4) absence of cracking in the speckle pattern during deformation before the testing ends, and (5) no interference from the speckle pattern on the material properties of the test sample.

In this study, speckle patterns were applied to the test articles using an airbrush. This method was selected for its ability to produce fine random speckle patterns suitable for the miniature test articles under investigation in this study. To achieve a high-contrast speckle pattern, a white background was first applied to the samples using a high-temperature paint. The samples with white paint were dried at room temperature for longer than 12 hours. Subsequently, a high-temperature black paint was applied on the test articles to create the speckle pattern. The quality of the pattern was inspected using a camera (FLIR Blackfly BFS-U3-27S5M) with a DistaMax lens (Model K2). Figure 5 shows two examples of speckle patterns on a WSTA and ISTA, highlighting the fine speckle details, random distribution, and good black-and-white contrast. Previous validation work (Mahajan et al. 2023) confirmed the accuracy of the speckle pattern by comparing DIC strain data with measurements from an extensometer and linear variable differential transformer (LVDT) during elevated-temperature tensile and creep tests. These extensive validation tests demonstrated the robustness and fidelity of the speckle pattern and DIC setup.

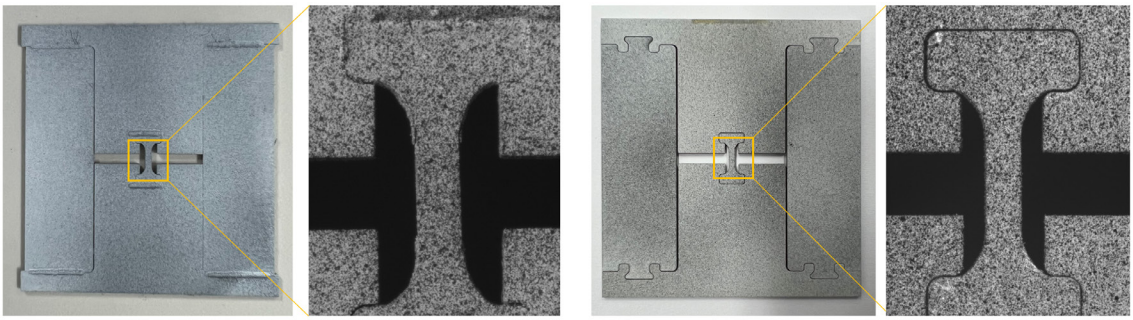

Figure 5. DIC speckle pattern prepared on (a) a WSTA and (b) an ISTA.

3.1.3. Testing Load Cycles

To evaluate the performance of the test articles, various temperature-cycling profiles were employed. Table 1 details the parameters for these temperature cycles, including peak and valley temperatures, ramp-up and ramp-down rates, and hold time at peak temperature. Temperature Profile A-1 involved a limited number (<50) of cycles and was designed to assess the strain range of the specimen under temperature variation. After validating the test-article design, intermediate (~350 cycles) and long-term (>1000 cycles) testing was conducted to investigate the strain-range evolution during creep-fatigue testing. The Profile A-2 included a 300 hours hold at a peak temperature of 700°C to examine strain evolution under steady-state conditions. Additionally, the C-1, C-2, and C-3 thermal-cycling experiments were performed with temperature variations between 400 and 700°C, incorporating different heating and cooling rates. These experiments aimed to study strain response relative to ramp rate to accommodate various reactor events and to accelerate the thermal-cycling process.

Table 1. Temperature profiles applied on surveillance test articles

Cycle Name	Peak Temp. (°C)	Valley Temp. (°C)	Ramp Up and Ramp Down Rates (°C/min)	Hold Time at Peak Temperature (hr)
A-1	700	500	8	0.5
A-2	700	35	5, (natural cool down)	300
C-1	700	400	12	0.5
C-2	700	400	7.5	0.5
C-3	700	400	3.33	0.5

3.2. Test Results

3.2.1. Welded Surveillance Test Article

A WSTA was used to evaluate the furnace heating setup and ensure high-quality imaging for DIC analysis, aiming for accurate and clean strain measurements. Figure 6a shows a WSTA sample mounted on a fixture for furnace heating. The speckle pattern was applied on the WSTA using an air-brush method to achieve high-resolution speckles across the specimen. Figure 6b displays the camera view of the WSTA, highlighting the gauge area for strain calculation. The WSTA underwent 10 thermal cycles from 500°C to 700°C with a heating and cooling rate of 10°C/min. After the final cycle, the specimen was cooled to room temperature with a programmed cooling rate of 10°C/min. A type K thermocouple was welded onto the Alloy 617 driver to monitor the temperature of the test article.

Figure 6c illustrates the strain response as a function of temperature. The image of the WSTA at room temperature served as the reference (zero strain) for strain calculation. As shown in Figure 6c, the furnace setup, combined with heat-haze mitigation strategies and the refined speckle pattern, resulted in a high signal-to-noise ratio for strain analysis. A strain range of 0.5% was observed during temperature cycling, which is consistent with the design (Mahajan et al. 2023). This test demonstrated the successful tracking of strain evolution using the furnace heating setup.

Figure 7a1–3 displays optical microscopy images of the specimen after cooling to room temperature. Notably, out-of-plane deformation was observed between the A617 drivers and 316H columns. This out-of-plane bending is expected as reported previously due to the significant compressive stress in the specimen after temperature ramp down (Mahajan et al. 2023). As a result of bending in the camera-furnace direction, a positive residual strain was measured when the test article cooled to room

temperature, as shown in Figure 6c. No visible cracking was observed near the specimen and welds after the 10-cycle thermal treatment.

The WSTA was then subjected to five additional thermal cycles, with a reduced heating and cooling rate of 8°C/min. Figure 6d plots the evolution of strain and temperature, with room-temperature strain set as the reference. The strain response exhibited a high signal-to-noise ratio, with a strain range of 0.47% during these cycles, comparable to the initial 10-cycle treatment. Figure 7b1–4 shows optical micrographs illustrating similar out-of-plane bending of the driver-column-specimen assembly upon cooling. Inspection of the welds under optical microscopy revealed no visible cracking. The testing with the WSTA demonstrated that:

1. The test article with a welding design can achieve expected strain range during thermal cycling, which is essential for damage assessment
2. The test article can effectively monitor strain response during typical reactor operations, including multiple ramp-up, steady-state, and ramp-down cycles
3. The strain range of the specimen during cycling can be accurately measured using the furnace heating setup and DIC technique
4. The test article can be removed from the furnace to assess accumulated damage and can be reinstalled in its designated location to continue damage accumulation.

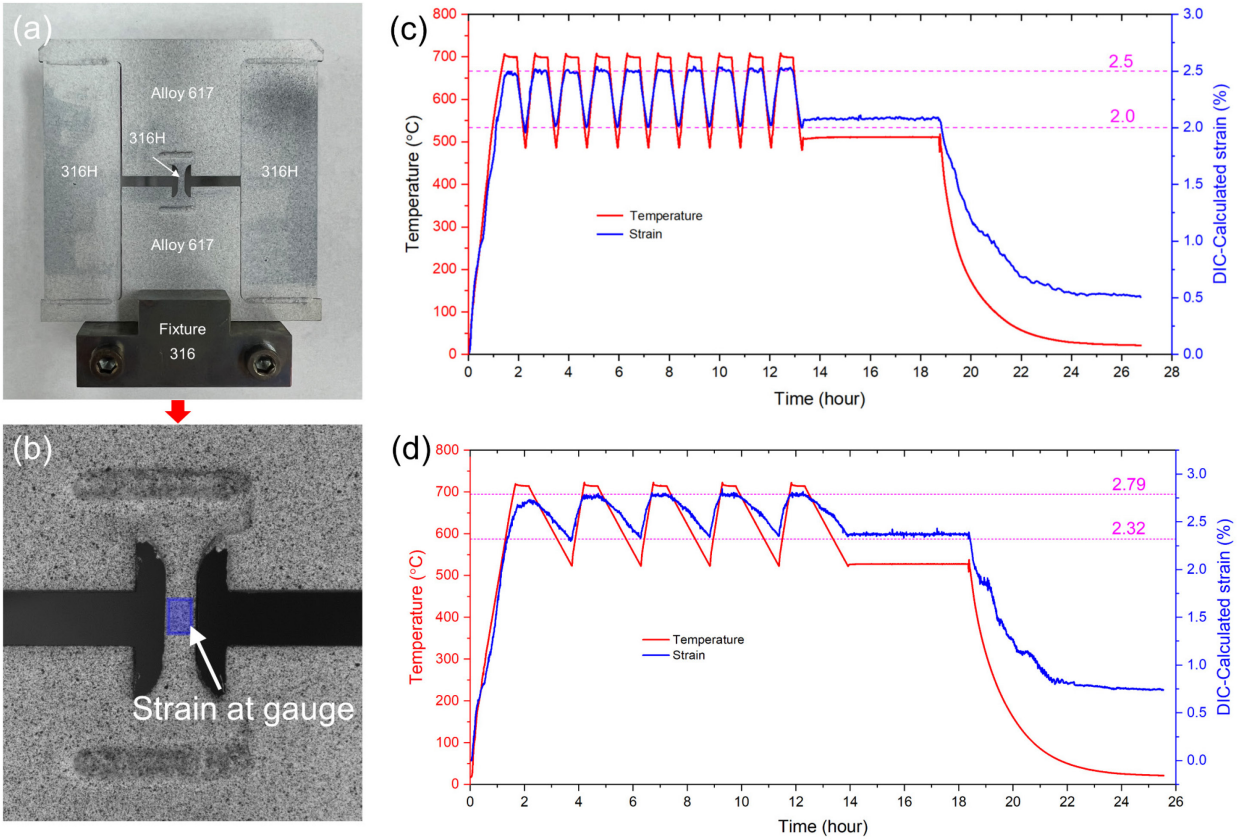

Figure 6. (a) A WSTA with prepared speckle pattern and (b) A reference DIC image. Strain and temperature evolution during (c) 10-cycle and (d) additional 5-cycle thermal treatment from 500 to 700°C.

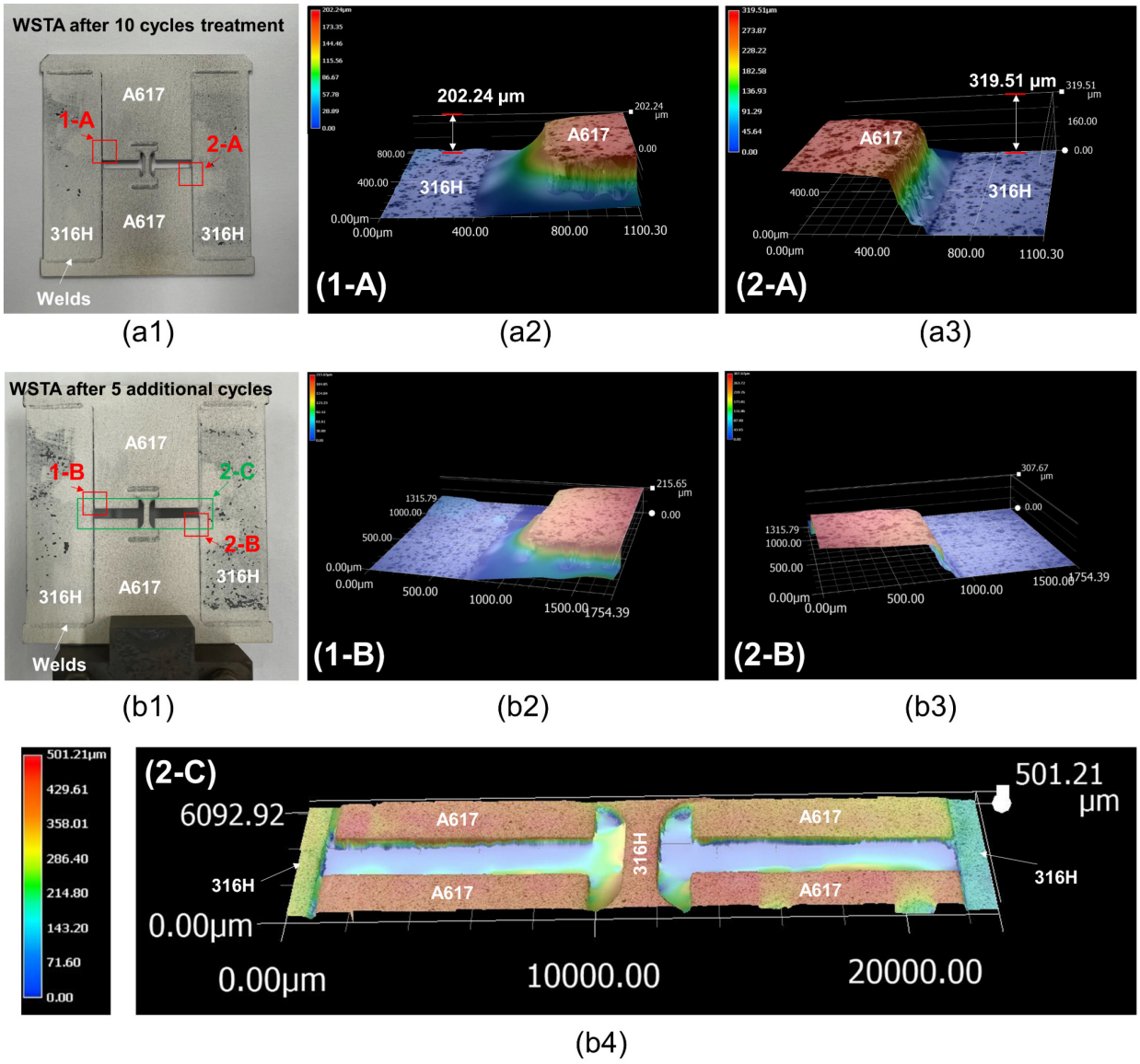

Figure 7. (a1) A WSTA after 10 cycles thermal treatment with two marked areas inspected by optical microscopy to show (a2, a3) out-of-plane deformation between the driver and column. (b1) A WSTA after additional five cycles thermal treatment with three marked areas inspected by optical microscopy to show (b2, b3, b4) out-of-plane deformation between driver-column-specimen assembly.

3.2.2. Cyclic Testing on WSTA

The results discussed in Section 3.2.1 validated the successful acquisition of strain evolution using the furnace heating and DIC setup. This validated setup was then used to conduct a mid-term cyclic test on a WSTA, applying thermal treatments from 500 to 700°C, with a heating and cooling rate of 8°C/min, a 30-minute hold at 700°C, and no hold at 500°C (Thermal Profile A-1). A total of 350 thermal cycles were performed on the WSTA over a duration of 500 hours. Figure 8 plots the temperature and strain profiles during the testing. The strain profile exhibits a clean profile. An initial increase in strain was observed due to cyclic strain hardening. The average strain range between peak and valley temperatures was 0.6%. Notably, there was no significant decrease in the strain range over the 350 cycles, which aligns with expectations given the limited number of cycles conducted on the test article.

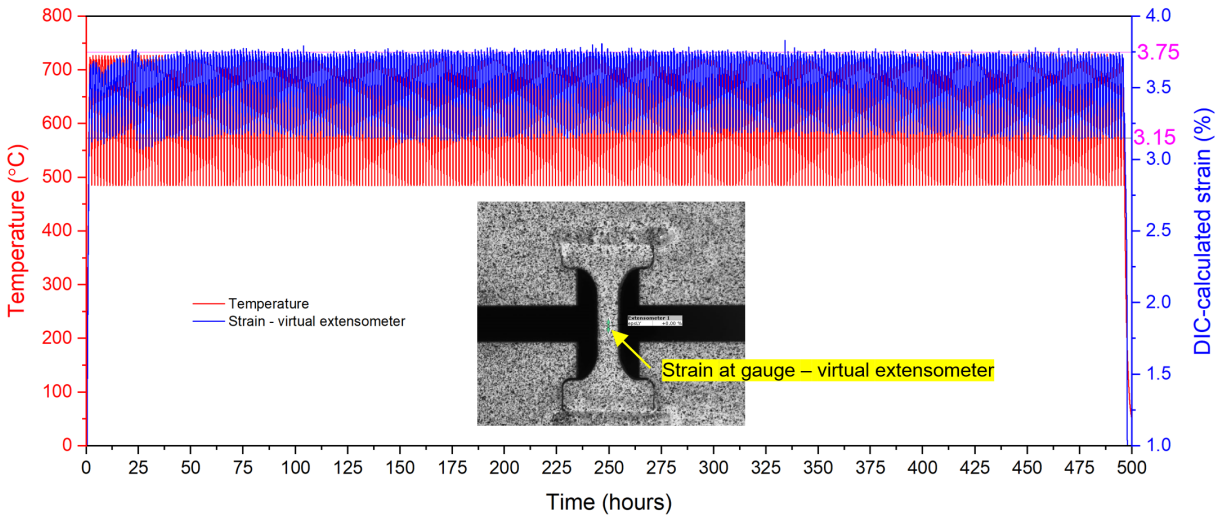

Figure 8. Temperature and strain profiles during a 350-cycle thermal treatment on a WSTA.

3.2.3. Test-to-Rupture Cyclic Test on WSTA

A long-term test-to-rupture cyclic test was conducted on a new WSTA to investigate strain response and assess the reliability of the welds at the driver-column-specimen joints. This test involved 1012 thermal cycles over 1484 hours. The test was terminated after 1012 cycles due to a low strain range observed between temperature cycles. Figure 9a and Figure 9b show the WSTA with its prepared speckle pattern prior to the test and an image obtained by the DIC camera, respectively. As depicted in Figure 9b, three virtual extensometers were used for strain calculation: (1) extensometer 1 at the gauge area, (2) extensometer 2 across the edges of the drivers, and (3) extensometer 3 across the welds of the specimen and driver. The image taken at room temperature was used as the strain-free reference. Figure 9c provides an overview of the temperature and strain evolution over the 1012 cycles, while Figure 10 offers a magnified view of different testing periods.

Figure 9c and Figure 10 reveal that the strain and strain range in the gauge area increased gradually during the initial five cycles from 500 to 700°C due to cyclic strain hardening under creep-fatigue testing. The strain range at the gauge remained relatively consistent at 0.55% for the first ~340 thermal cycles (500 hours). After 500 hours, a continuous decrease of strain range was observed. The strain range gradually declined to 0.27% and kept relatively constant till the end of the test. The flat strain profile near 1,450 hours (Figure 9c) is due to the maximum number of cycles (999) that could be programmed into the furnace. The furnace program was restarted to continue thermal cycling beyond 999 cycles. The observed decline in strain range with increasing cyclic number suggested potential cyclic strain softening of the specimen. However, strain profiles across the specimen-driver joint (welds) indicated potential weld failure that lead to the decreased strain range of the specimen. Figure 9c shows that the strain across the welds (virtual extensometer 3) exhibited a gradual increase of strain range after 500 hours of cyclic testing, corresponding to the time frame when the strain range at the specimen gauge decreased. This increase in strain range at the welds may indicate possible weld failure, leading to reduced stress/strain at the gauge. The strain range across the A617 drivers (green curve for extensometer 2 shown in Figure 9c) is calculated by tracking the two corner points on drivers as shown in Figure 9b. Driver material between weld lines and the corner is not subjected to any external load. Thus, relative deformation of weld lines between drivers and specimen, is captured by the deformation of driver corners. DIC uses initial length between driver corners and not the initial distance between welds, to calculate the strain as shown by extensometer 2. Therefore, strain values from extensometer 2 are higher compared to the strain measured in the gauge section. This information is useful to calculate the deformation between weld lines between drivers and specimen, which could be used to calculate strain in the specimen.

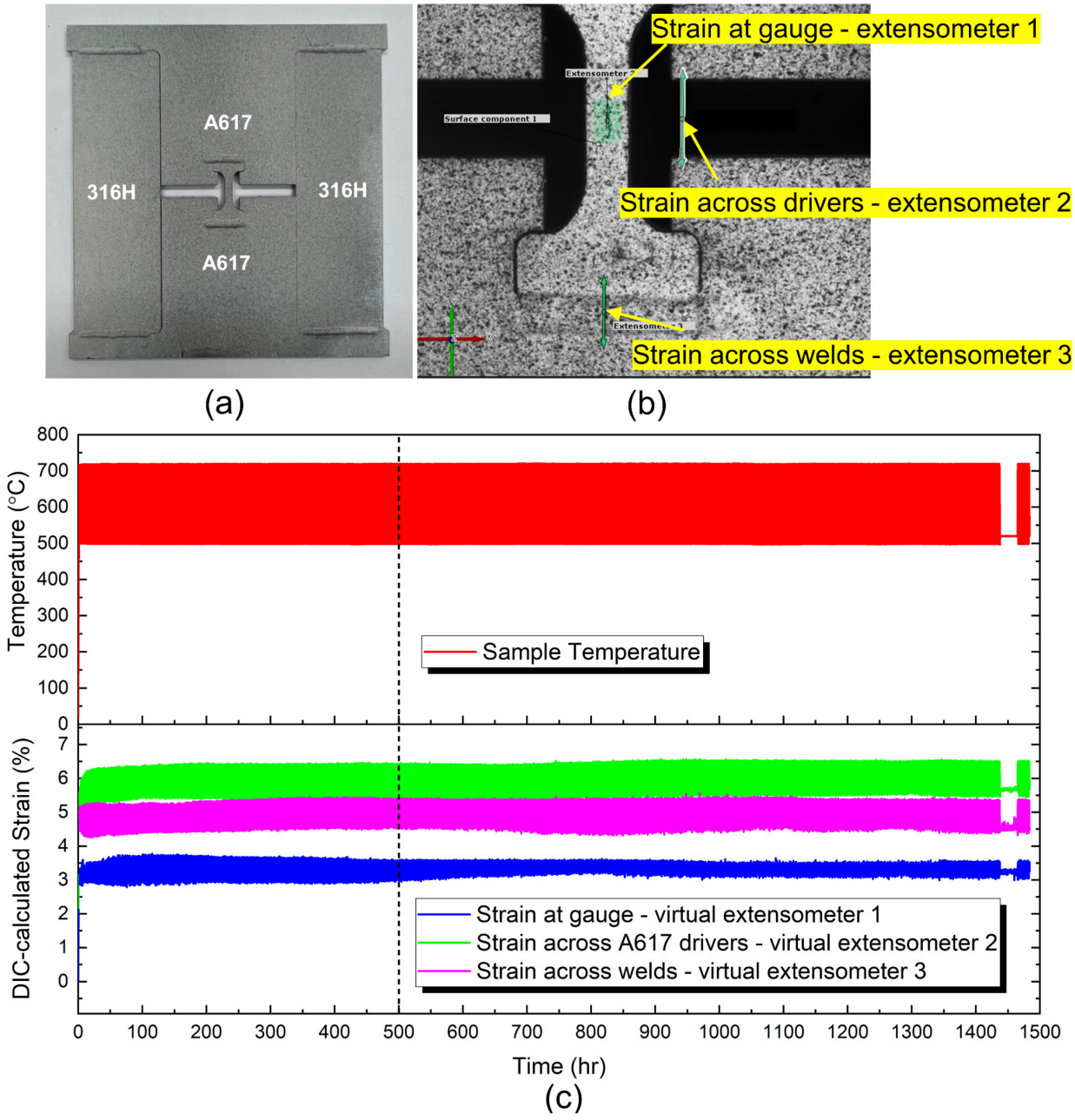

Figure 9. (a) A WSTA prepared with speckle pattern for test-to-rupture cyclic test. (b) A DIC image of the WSTA with three extensometers (at gauge, across drivers, and across welds) marked on the DIC image. (c) Temperature and strain profiles during a 1012-cycle cyclic test on a WSTA where change of strain range was observed at the time frame of 500 hours.

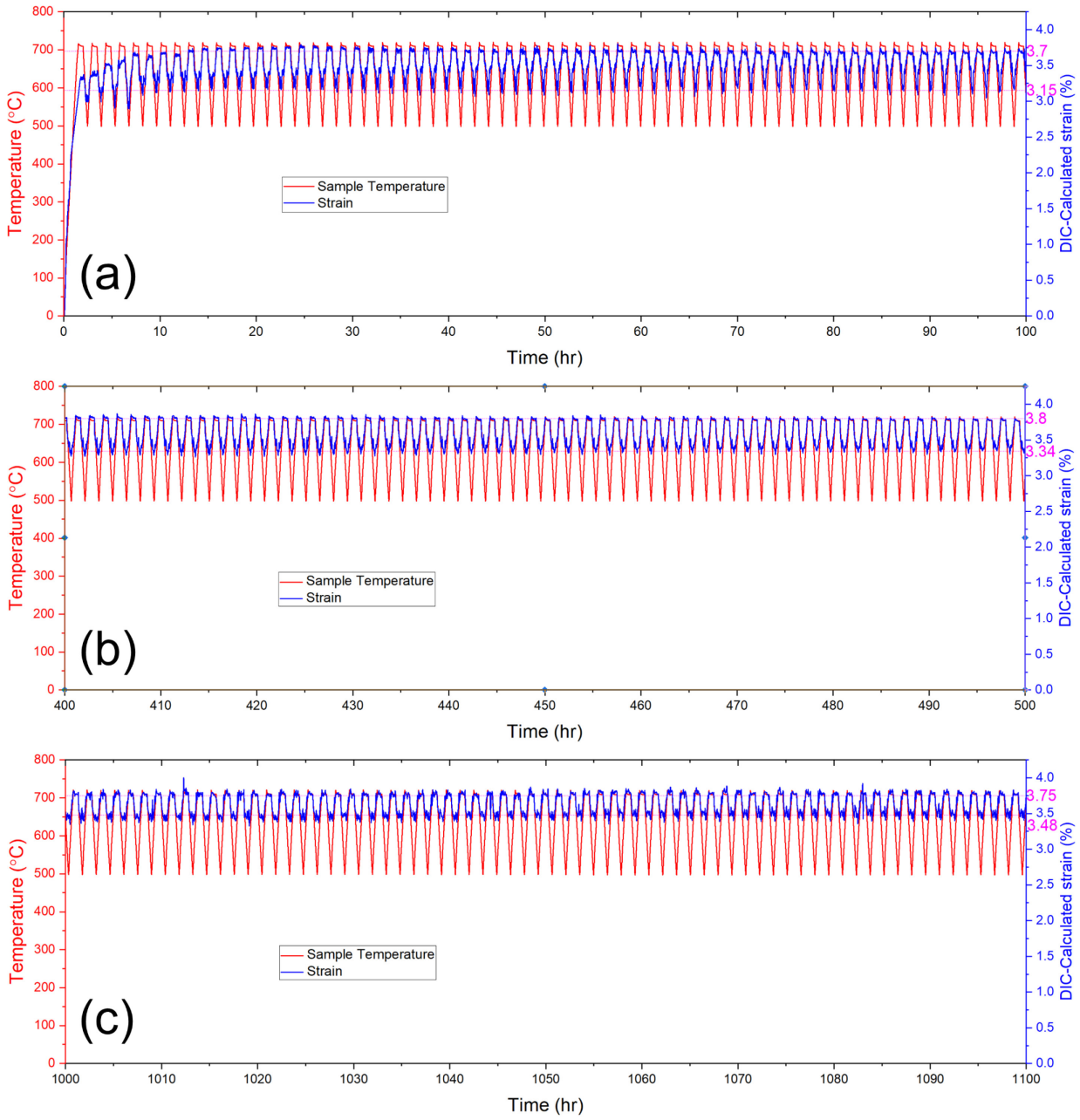

Figure 10. Test-to-rupture cyclic testing on WSTA showing segments between (a) the initial 100 hours with a strain range of 0.55%, (b) 400 to ~500 hours with a strain range of 0.46%, and (c) 1000 to ~1100 hours with a strain range of 0.27%.

X-ray computed tomography (XCT) scans were performed on the post-test WSTA to assess the integrity of the welds after 1012 cycles of cyclic testing. Figure 11a displays XCT images of the sub-volume near the welds. It can be observed that a cluster of microcracks at both the top and lower welds were seen. These cracks developed during the prolonged cyclic loading. Because of these microcracks, strain over the welds shows a gradual increase after 500 hours of cycling (Figure 9c), which also resulted in the decline of strain range over the specimen gauge section. The welds in the test articles were prepared using directed energy deposition (DED) with SS316 as the filler material. To enhance weld quality, efforts should be pursued on optimizing key DED parameters and exploring alternative filler materials.

Additionally, XCT evaluation of welds prior to thermal cycling is needed to establish baseline properties. Further investigation of weld performance under irradiation and molten salt environment is also necessary to ensure weld reliability. Figure 11b shows the XCT images of the material at the gauge, where a few lines are visible. These lines may indicate potential microcracks or could be artifacts of the XCT instrument. A destructive evaluation to further characterize the material at the gauge was not performed, as the specimen was machined from the test article for a creep test using a creep load frame (Case 2 in Figure 3) to evaluate the remaining creep life of the material.

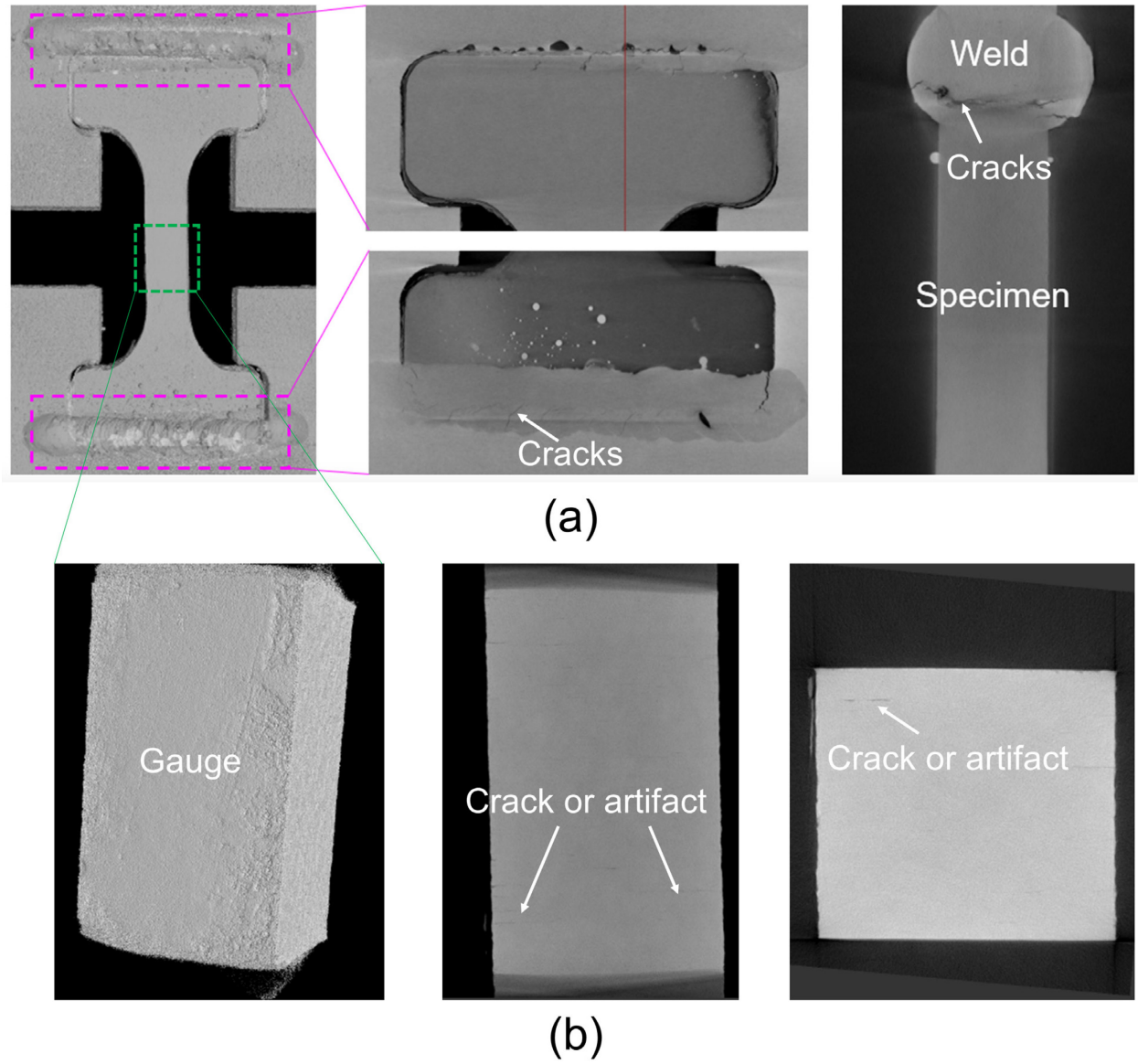

Figure 11. XCT images illustrating the subvolumes of the post-test-to-rupture WSTA (a) near welds with cracks and (b) at the gauge.

3.2.4. Post-Test-to-Rupture Creep on WSTA

The WSTA that underwent 1012 cycles was machined to obtain the specimen-driver assembly for creep testing using a standard-creep load frame. Creep testing was conducted at 700°C under a stress of 130 MPa. Under this condition, the expected creep life of the material is 300 hours. The specimen was gripped at the driver regions, as shown in Figure 12a. Speckle patterns were applied to the specimen for DIC strain monitoring. To ensure proper alignment of the specimen within the creep frame, holes were machined in the driver sections to align with the pins in the creep grips. Figure 12b presents the creep-strain curve, which shows that the specimen ruptured at 60.6 hours, significantly shorter than the anticipated 300-hour creep life. The fracture occurred in the gauge region, as depicted in Figure 12a. Although reduced creep life is expected due to damage accumulation during cyclic loading, bending and twisting of the specimen during loading into the creep frame may attribute additional damage. The miniature specimen design is sensitive to the bending and torsion stresses induced due to misalignment. Future effort will focus on optimizing sample alignment and loading conditions to improve the accuracy of creep testing.

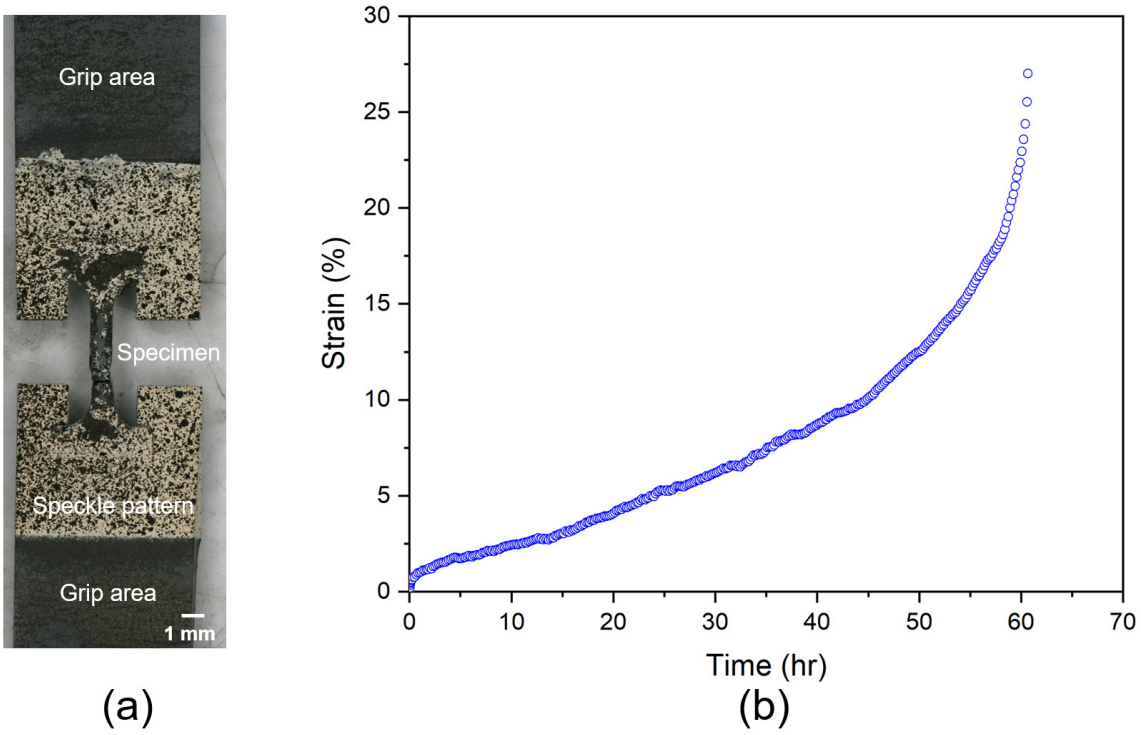

Figure 12. (a) An image of the fractured specimen after creep test. (b) Strain profile during creep test on the specimen that has experienced 1012-cycle thermal treatment.

3.2.5. Interlocking Surveillance Test Article

A pristine ISTA was tested using the furnace setup to investigate its strain response under thermal cycling. Figure 13a shows the ISTA with speckle patterns prepared using airbrush. A Type K thermocouple was welded on the driver adjacent to the specimen to monitor the temperature during the test. The thermal treatment applied consisted of 10 cycles from 500 to 700°C with a heating and cooling rate of 10°C/min, a 30-minute hold at 700°C, and no hold at 500°C.

The ISTA was designed and machined using electric discharge machining (EDM) to ensure a tight fit between drivers, columns, and specimen. This design eliminates the need for welding at the driver-column-specimen connections, which is an advantage of ISTA. This is because it enables the use of

materials that are challenging to weld, with higher CTE mismatch that can reduce the overall dimensions of the test articles, such as refractory alloys (Mo, Ta, and W alloys) and even ceramics. As cracks were observed in the welds of the WSTA after 500 hours of thermal cycling (Figure 11a), the interlocking design also assures improved reliability of the test articles under prolonged testing for materials surveillance. Moreover, welding-free design can eliminate welding failure during testing in reactors where, not only cyclic mechanical load, but also irradiation and corrosion environments pose significant challenges to welds. However, one challenge with interlocking design is that it requires high machining tolerances (gap-free connections at driver-column-specimen joints) so that the strain under temperature variations can be fully engaged on the specimen. Additionally, the ISTA should remain flat during loading/unloading and testing because misalignment of the assembly could lead to strain inaccuracy.

Figure 13d illustrates the strain evolution at different areas of the ISTA: (1) in the gauge area (DIC subset at specimen shown in Figure 13c), (2) across the edges of the drivers (Virtual Extensometer 1), and (3) across the gaps between specimen and drivers (Virtual Extensometers 2 and 3). The subset-based DIC method was used to measure average strain over the gauge area while virtual extensometers were employed for DIC analysis at the drivers and gaps. The image taken at room temperature was used as the (strain-free) reference image. The strain profiles shown in Figure 13d demonstrated high signal-to-noise ratio. The strain range in the gauge area between peak and valley temperatures was 0.42% and the maximum strain (thermal strain + mechanical strain) on the specimen is 1.58%. This maximum strain and strain range are lower than expected based on the test article design and the WSTA results, likely due to microgaps at the driver-column-specimen joints.

The presence of these microgaps meant that some of the strain during the initial temperature ramp-up was absorbed by the gaps rather than being applied to the specimen, leading to reduced overall strain. This observation is corroborated by the low strain ranges observed with Virtual Extensometers 2 and 3 (across the driver-specimen gaps), which indicate the presence of gaps. Specifically, Extensometer 2 shows a significant negative strain (-1%) upon cooling, suggesting a reduction in gap size, while Extensometer 3 shows a positive strain of 1.2% upon cooling, indicating an increase in gap size at the lower specimen-driver interlocking joint. These results suggest that the ISTA has gaps at the driver-column-specimen joints due to limited tolerance of the EDM machining. To improve interlocking design, machining optimization is necessary, and partial spot welding at the joints may further ensure that the strain induced by CTE mismatch is fully applied to the specimen.

Figure 14 shows optical microscopy images of the ISTA after thermal cycling, highlighting the out-of-plane deformation of the A617 drivers relative to the 316H columns. The observed deformation, less than 57 μm, is minimal compared to those seen in the WSTAs. This reduced deformation is attributed to the initial gaps in the driver-column-specimen joints, which absorbed the residual strain in the specimen and consequently resulted in less out-of-plane bending of the interlocking test article.

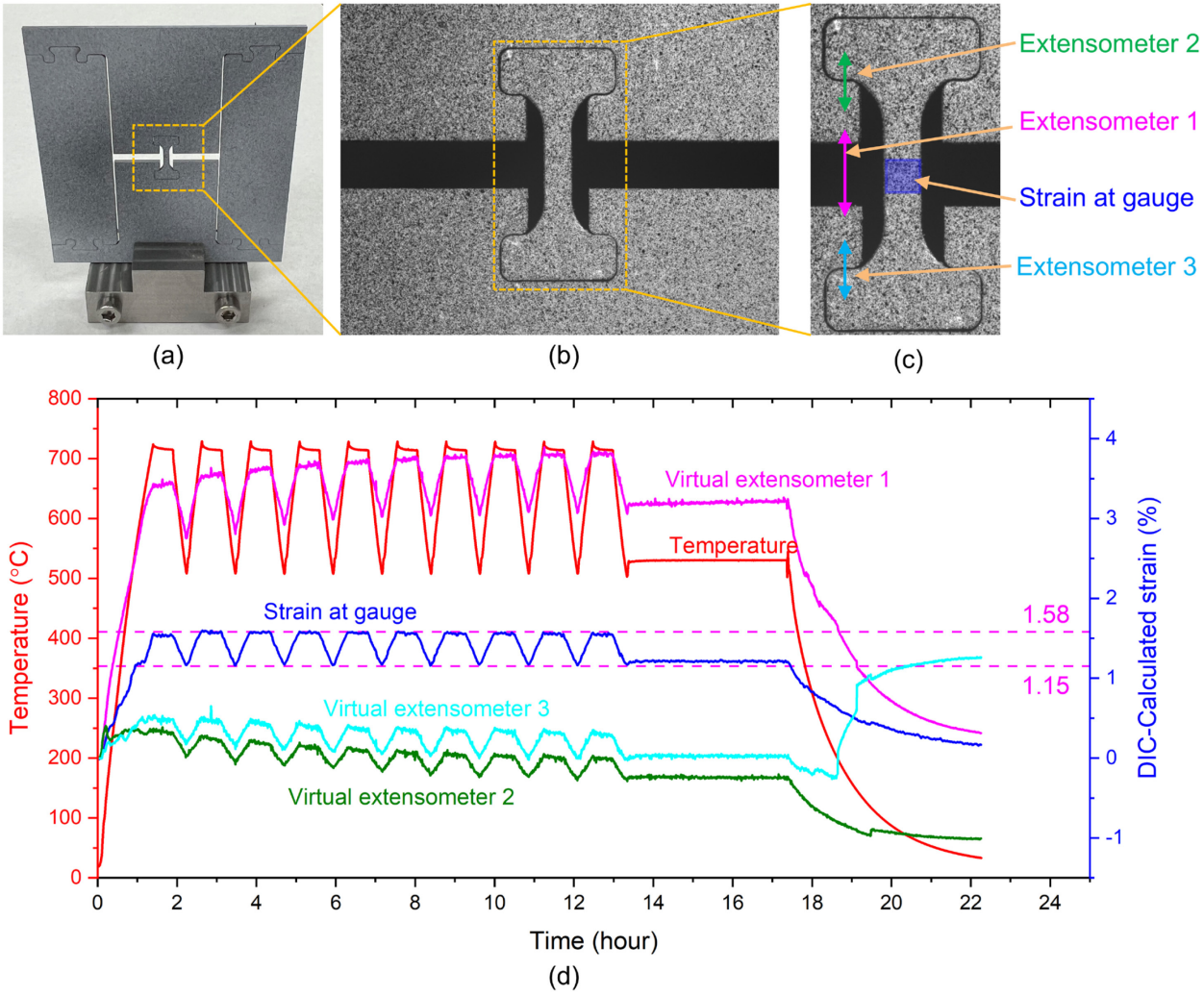

Figure 13. (a) A pristine ISTA with prepared speckle pattern. (b) A reference image recorded by the DIC camera. (c) Enlarged view of the area of interest with subset area at gauge and virtual extensometers over gaps and drivers. (d) Temperature and strain profiles from 10-cycle thermal treatment on an ISTA.

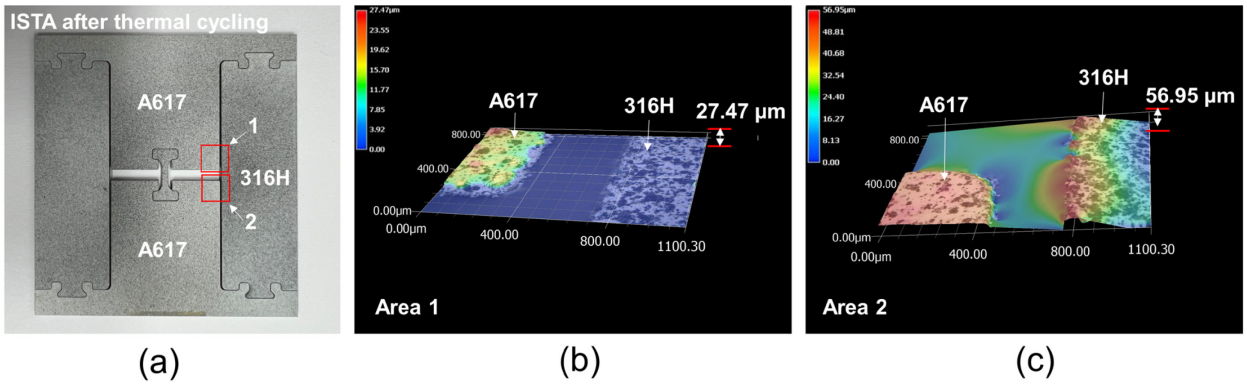

Figure 14. (a) A post-test ISTA with two areas inspected by optical microscopy to show (b, c) out-of-plane deformation between A617 driver and 316H column.

3.2.6. Creep at 700°C on WSTA

Creep testing was conducted on a test article with a 300-hour hold at 700°C (Profile A2 in Table 1) to examine the strain response under constant temperature. Figure 15 shows the strain profile throughout the testing period. The specimen gauge area recorded a total strain of 3.6% with no obvious change observed over the 300-hour test. The noise during the dwell period is attributed to the use of a different tube furnace, as the original furnace was reserved for the long-term test-to-rupture cyclic testing. This alternative furnace may introduce more vibrations to the test article, which likely contributed to the noise. Additionally, out-of-plane deformation between the driver and column was noted as a result of the residual compressive strain on the test article upon cooling (Mahajan et al. 2023).

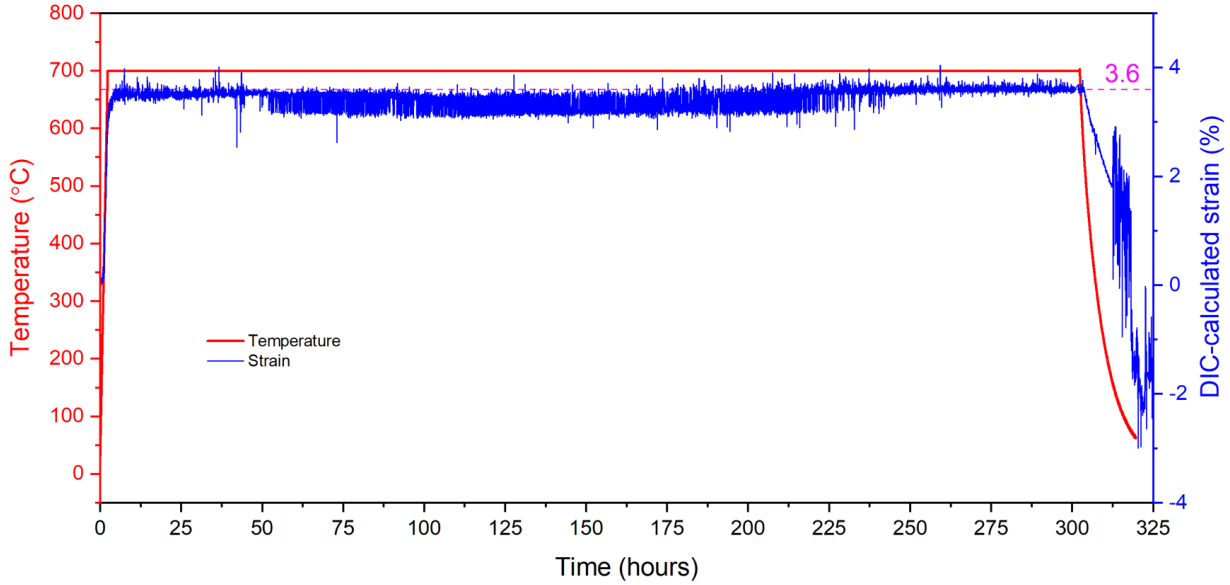

Figure 15. Strain and temperature profiles for a creep testing with 300 hours dwell at 700°C on a WSTA.

3.2.7. Multi-Profile Cyclic Test on WSTA

A multi-profile cyclic test was performed on a WSTA using thermal profiles C-1, C-2, C-3, and A-2. Profiles C-1, C-2, and C-3 featured varying heating and cooling rates to assess strain response as a function of these rate. Figure 16a and Figure 16b display virtual extensometers placed at the specimen gauge and across the drivers, respectively. The strain evolution at specimen gauge is shown in Figure 16c while the strain response across the drivers is plotted in Figure 16d. As illustrated in Figure 16a, a gradual increase in strain was observed under thermal profile C-1, attributed to cyclic strain hardening. The strain range between peak and valley temperatures is 0.67%, encompassing both thermal and mechanical strain. After completing Profile C-1, testing proceeded with Profile C-2, which featured a reduced heating and cooling rate. The peak-valley strain and strain range for C-2 were similar to those obtained with C-1. Profile C-3, which employed an even-slower heating and cooling rate yielded strain and strain range results consistent with C-1 and C-2. These results suggest that variations in heating and cooling rates have minimal impact on the strain response, demonstrating the robustness of the test article design for monitoring material degradation across different reactor temperature variance events. Typical temperature-ramp rates in reactors are slower than the temperature ramp rates used in this study. Temperature-ramp-rate evaluation also established that the fast temperature ramps used in the laboratory furnace setup are acceptable to evaluate test article performance.

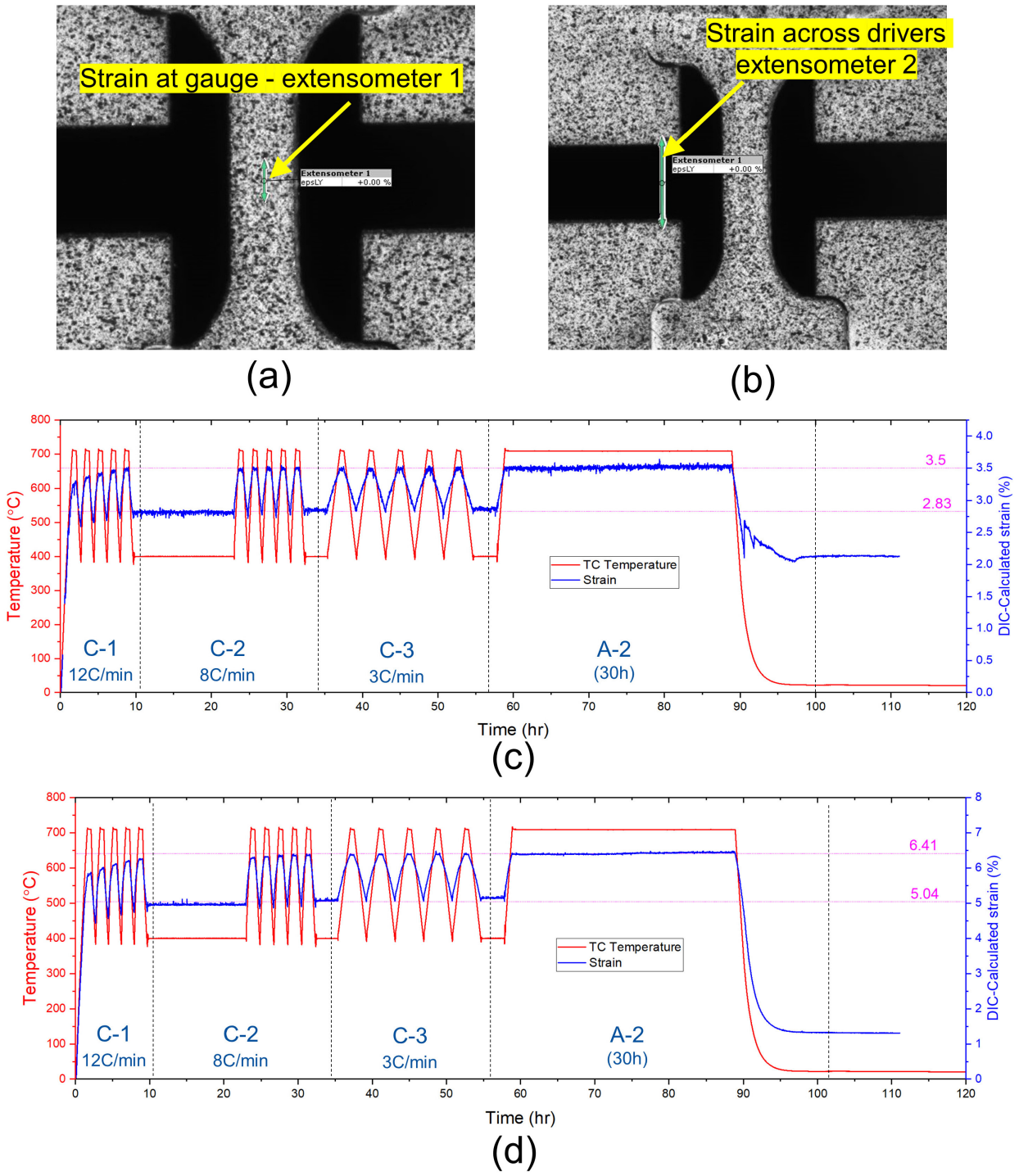

Figure 16. DIC images of WSTA with strain at (a) gauge and (b) across drivers. Evolution of strain at (c) gauge and (d) across welds during multi-profile cyclic testing on a WSTA.

3.2.8. Interlocking Design with TZM and Alloy 709

An interlocking design incorporating titanium-zirconium-molybdenum (TZM) and Alloy 709 was tested in this research. A detailed description of the TZM-A709 test article design is provided in a previous report (Mahajan et al. 2023). TZM and Alloy 709 exhibit a high CTE mismatch, which facilitates a reduction in the overall size of the test article. However, TZM is susceptible to severe oxidation at elevated temperatures. To prevent this, the test article was enclosed in a glass capsule filled with argon. The glass capsule was loaded into a tube furnace for thermal treatment while the strain of the specimen was monitored using DIC. During initial testing, it was noted that the speckle pattern lost acceptable contrast at high temperatures due to the off-gassing from the paint within the glass capsule. To address this issue, the A709 specimen, with speckle pattern, was heat-treated in air at 700°C for 30 minutes to expel chemicals from the paint before being assembled with TZM. A four-cycle thermal treatment was then performed on the TZM-A709 test article using Profile A1 (refer to Table 1). Figure 17 exhibits the temperature and strain history from this testing. Both subset and extensometer methods were employed for strain analysis. Despite the poor contrast of the speckle pattern at elevated temperatures, DIC analysis provided acceptable strain values. Future efforts will focus on exploring alternative materials for drivers to improve strain accuracy, encouraging testing possibilities in air to enhance DIC imaging quality and minimize experimental procedures while further minimizing the dimensions of the test article.

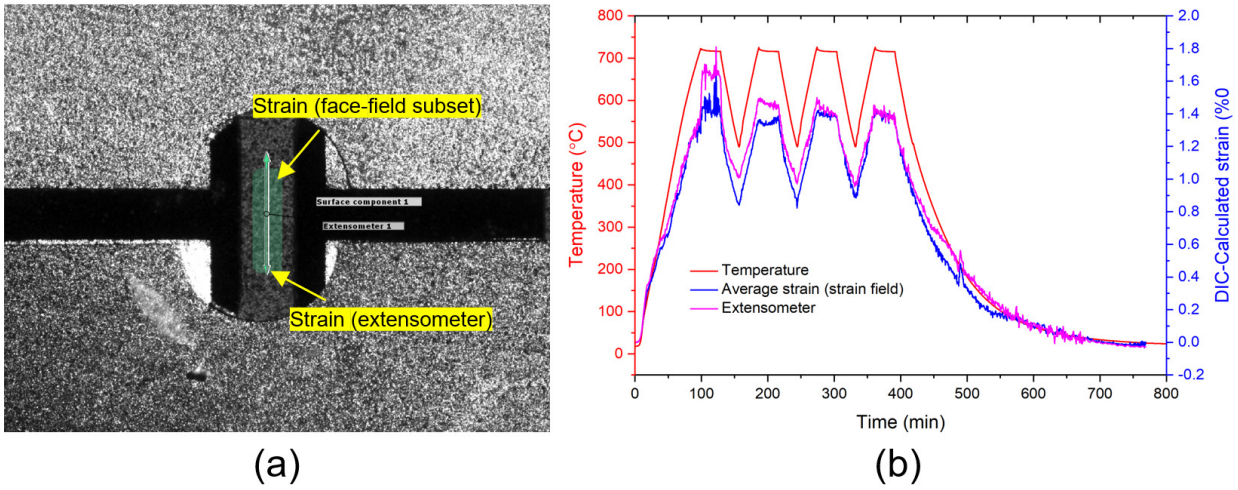

Figure 17. (a) A DIC images of a TZM-Alloy 709 interlocking design encapsuled in a glass capsule. (b) Temperature and strain history during thermal cycling.

4. SUMMARY AND FUTURE WORK

Monitoring material degradation due to the combined effects of corrosion, irradiation, and mechanical loading is critical to ensure the reliable performance of reactor components. This report details the design, fabrication, and testing of surveillance test articles aimed at assessing material damage in reactor-relevant environments for effective degradation management. Both welded and interlocking test articles with reduced sizes were developed and evaluated. Key findings from this study include:

1. The welded test article design successfully captured the expected strain range during thermal cycling (500–700°C) using a tube-furnace heating setup and DIC technique. The interlocking design requires improved machining tolerance to engage strain coupling in the test-article assembly.
2. A 500-hour thermal-cycling test on WSTA exhibited a stable strain range of 0.6%. However, a ~1500-hour cyclic test revealed a gradual decrease in strain range after ~500 hours, with an increase in strain range observed across the specimen-driver welds. XCT examination confirmed the presence of microcracks in the welds after testing, indicating weld failure after long-term cycling. Efforts are underway to optimize welding conditions and filler materials selection to enhance weld quality.
3. Creep testing on a specimen from the WSTA after ~1500 hours of cyclic testing, conducted using a standard creep frame, revealed a short creep life, attributed to the sensitivity of the SSJ specimen to stress from testing setup.
4. A 300-hour creep test at 700°C on WSTA showed no noticeable change in strain. Multiprofile cyclic testing revealed consistent strain responses, demonstrating that the surveillance test articles can effectively capture damage from various reactor thermal events.

Planned work for FY-25 includes:

1. Welding optimization: improve welding parameters and filler-material selection to enhance weld quality for the welded test article design. XCT evaluation of welds before and after thermal cycling will be conducted to assess the weld performance under cyclic loading.
2. Thermal cycling in molten salt: conduct thermal cycling tests in a molten-salt environment to simulate damage from mechanical loading and corrosion. Baseline tests without salt exposure will be performed to differentiate damage caused by corrosion.
3. Driver-material selection: explore the use of refractory metals as driver materials to reduce the overall size of test articles and/or increase of the stress applied to the specimen due to larger CTE mismatch between driver and specimen.
4. Furnace-testing validation: validate test-article designs with refractory-metal driver materials and weld materials using the furnace-heating approach. Simultaneous testing of multiple test articles in one furnace will be pursued to increase the throughput of cyclic testing.

5. REFERENCES

ASME. 2023. “BPVC Section III-Rules for Construction of Nuclear Facility Components-Division 5-High Temperature Reactors.” Boiler and Pressure Vessel Code, American Society of Mechanical Engineers, New York, NY.

ASTM International. 2024. “Standard Practice for Surveillance Testing of High Temperature Nuclear Component Materials.” E531-23, American Society for Testing and Materials.

Mahajan, H. P., et al.. 2023. “Development of Surveillance Test Articles with Reduced Dimensions and Material Volumes to Support MSR Materials Degradation Management.” INL/PRT-23-74540, Rev 0, Idaho National Laboratory, Idaho Falls, ID. https://www.osti.gov/biblio/1999988.

McMurtrey, M. D., et al. 2022. “Phase II Development of the Surveillance Test Articles to Improve the Design, Fabrication, and Testing.” INL/RPT-22-69281, Idaho National Laboratory, Idaho Falls, ID. https://www.osti.gov/biblio/1906467.

Messner, M. C., and T. -L. Sham. 2021. “Preliminary Procedures and Acceptance Criteria for in situ Structural Materials Surveillance for MSR.” ANL-ART-229, Argonne National Laboratory, Lemont, IL. https://www.osti.gov/biblio/1817876.

Messner, M. C., Y. Momozaki, and E. Boron. 2022. “Report on Thermal Cycling Testing and Bimaterial Weld Development for a Passively Actuated Materials Surveillance Test Article.” ANL-ART-245, Argonne National Laboratory, Lemont, IL. https://www.osti.gov/biblio/1846247.

Messner, M. C., et al. 2021. “Fabrication and Testing of Two Passively Actuated Creep-Fatigue Surveillance Test Articles.” ANL-ART-228, Argonne National Laboratory, Lemont, IL. hhttps://doi.org/10.2172/1822414.

Messner, M. C., et al. 2020. “Initial development of an in situ, passive material surveillance test article for monitoring high temperature reactor structural components.” ANL-ART-198, Argonne National Laboratory, Lemont, IL. https://doi.org/10.2172/1660408.

U.S. Nuclear Regulatory Commission. 2023. “Material Compatibility for Non-Light Water Reactors.”- Draft Interim Staff Guidance, Document number 2023-04577. Accessed September 23, 2024. https://www.federalregister.gov/documents/2023/03/07/2023-04577/material-compatibility-for-non-light-water-reactors.

Wang, Y., T.-L. Sham, and R. I. Jetter. 2014. “Alloy 617 Creep–Fatigue Damage Evaluation Using Specimens With Strain Redistribution.” J*ournal of Pressure Vessel Technology* 137(2): 021402. https://doi.org/10.1115/1.4028054.